

A new radial basis integration method applied to the boundary element analysis of 2D scalar wave equations

A. Narváez^{*}, J. Useche

Universidad Tecnológica de Bolívar, Cartagena, Colombia

ARTICLE INFO

Keywords:

Domain integration
Boundary element method
Radial basis integration method
Dual reciprocity boundary element method (DR-BEM)
Scalar wave equation

ABSTRACT

A new integration method named the Radial Basis Integration Method (RBIM) that include the Kriging Integration Method (KIM) Narváez and Useche (2020) as a particular case and performs boundary only offline precomputations for the creation of a meshless quadrature was developed for its application in boundary elements. Herein, as in DR-BEM, the inertial term is approximated using radial basis functions, however, its particular solution is not needed. The quadrature is now obtained in a simpler way than in KIM, because the evaluations of domain integrals necessary to compute the weights of quadrature points, is done transforming those to the boundary instead of using the Cartesian Transformation Method. Using RBIM, weakly singular domain integrals may be computed with good accuracy over complex domains. The results obtained in some scalar wave propagation problems using both Houbolt- α and Newmark- α time marching methods show that this procedure can be even more accurate than other used in BEM analysis.

1. Introduction

Scalar wave propagation problems are commonly encountered in various engineering disciplines. For the case of interior problems based on a direct BEM formulation in which a fundamental stationary solution is used in combination with direct time integration algorithms, several strategies have emerged for the treatment of the inertial domain integrals that appear there. The first method used to solve these integrals is the Cell Integration Method (CIM), where a domain partition into simpler regions called cells is made. Its use with boundary elements is known as classic BEM [1–3]. With the idea of obtaining integral formulations that only involve boundary integrals, new methods have been developed, among these there are some with an approach similar to CIM but with the difference that they do not require a mesh fitting task, rather they use a Cartesian grid for integration purposes [4–6]. In the second instance, we can chronologically name those combined with BEM that convert domain integrals into boundary ones, among them we have: The Dual Reciprocity Method (DR-BEM) [7–13], the Triple Reciprocity Method (TR-BEM) [14,15], the Multiple Reciprocity Method (MR-BEM) [16–19], the Radial Integration Method (RI-BEM) [20], the Direct Interpolation with Boundary Elements (DI-BEM) [21] and more recently the Line Integration Method (LIM). The first three are based on the reciprocity theorem. In contrast to DR-BEM, MR-BEM only needs boundary collocation points, however, its application is restricted to certain types of problems. RIM is characterized by converting the domain integrals into boundary ones by previously carrying out an one

dimensional inner integral. It has the advantage of being able to eliminate some types of singularities in the integrand [22], however, the method becomes computationally inefficient when the radial integral cannot be computed analytically. LIM has the advantage that it only needs to evaluate integrals on lines generated from integration points located in the boundary elements, although it must be combined with Fast methods in order to be more efficient and approximate. DI-BEM unlike RI-BEM and LIM always allows the exact transformation to the boundary of domain integrals using a primitive radial basis function (for which there are no restrictions on its choice) in combination with Green's theorem.

On the other hand, within the category of methods based on meshless techniques, the following stand out: The Monte Carlo Method (MCM) [23,24], The Quasi-Monte Carlo Method [25], The Cartesian Transformation Method (CTM) [26] and The Kriging Integration Method (KIM) [27]. All of them are based on a quadrature defined for integration points distributed within the domain, however, except in the CMT such distributions can be random and allow solving problems with singularities without any special treatment, although in KIM this only seems to be true for weak singularities. All these methods can evaluate integrals on irregular domains with multiple boundaries. Moreover, regarding efficiency by taking into account the precision vs the number of integration points, KIM is as good as CTM even with fewer points and therefore it saves computational time in the integral evaluation process.

^{*} Corresponding author.

E-mail addresses: anarvaez@utb.edu.co (A. Narváez), juseche@utb.edu.co (J. Useche).

In BEM the discretization process for the domain and/or the boundary gives rise to a matrix equation of motion which is solved using several time marching stepping algorithms. When solving wave propagation problems, Houbolt [28] and Newmark [29] are the most common used methods. However, exist another stable and accurate alternatives [2,30–33].

Making a review of the different existing domain integration methods in dynamic problems, it is evident that no extensive studies has been carried out with RI-BEM to address scalar wave propagation problems. Only has been reported a new integration procedure incorporated into RI-BEM (hereafter referred as MRI-BEM) to analyze some problems in both convex and concave domains [34]. This approach uses an auxiliary point, conveniently located so that the function to be integrated in the radial direction is always evaluated over intervals within the domain. Although what is observed is that there are more application of RI-BEM related to acoustic eigenvalue and Helmholtz problems [35–37]. Similarly, the Triple reciprocity method (TRM) and DI-BEM has been applied to solve Helmholtz problems in [15,21], respectively.

As it has been noted, there are few methods in BEM to compute domain integrals that appears in applications concerning scalar wave equation problems.

In this paper, a meshless-based integration method as in [26,27,38], named the Radial Basis Integration Method (RBIM) has been developed for the computation of inertial domain integrals that are found in the BEM formulation of the 2D scalar wave equation. Using this quadrature, it is possible to compute them directly, therefore, it is a potential alternative in relation to the existent methods. The coupling between RBIM and BEM will be named RBI-BEM.

The other sections of this article are organized as follows: In the next section, the boundary integral representation of the scalar wave equation is shown. In the third section, the basis of the Radial Basis Integration Method is revised. In the fourth section, a review of the modified version of Radial Integration Method is performed. In the section fifth, in order to implement this method several subroutines are given as possible options . In section six, RBI-BEM is applied to solve some benchmark problems and comparisons with DR-BEM and the MRI-BEM are made. Finally, in section seven, some conclusions are presented.

2. Boundary integral representation of the scalar wave equation

The equation that governs transient scalar waves in the region Ω discarding source terms is (Fig. 1):

$$\nabla^2 u(\mathbf{x}, t) = \frac{1}{c^2} \frac{\partial u^2(\mathbf{x}, t)}{\partial t^2} \quad (1)$$

where c refers to the wave propagation velocity, $u(\mathbf{x}, t)$ represent the potential field variable, and t is the time.

The time dependent boundary conditions are defined as follows:

$$u(\mathbf{x}, t) = \bar{u}(\mathbf{x}, t), \quad \text{on } \Gamma_u \quad (2)$$

$$\frac{\partial u(\mathbf{x}, t)}{\partial n} = \bar{q}(\mathbf{x}, t), \quad \text{on } \Gamma_q \quad (3)$$

where n stand for the boundary outward normal. Additionally we have the following initial values:

$$u(\mathbf{x}, 0) = u_0(\mathbf{x}), \quad \text{on } \Omega \quad (4)$$

$$\dot{u}(\mathbf{x}, 0) = \dot{u}_0(\mathbf{x}), \quad \text{on } \Omega \quad (5)$$

The boundary element formulation for Eq. (1) is defined as follows [39]:

$$c(\xi)u(\xi) + \int_{\Gamma} \bar{q}^*(\xi, \mathbf{x})u(\mathbf{x})d\Gamma = \int_{\Gamma} u^*(\xi, \mathbf{x})q(\mathbf{x})d\Gamma - \frac{1}{c^2} \int_{\Omega} u^*(\xi, \mathbf{x})\ddot{u}(\mathbf{x})d\Omega \quad (6)$$

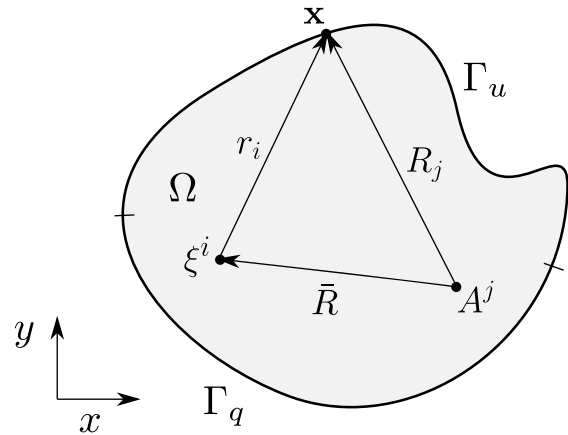


Fig. 1. Physical domain, its boundary and some point relationships.

where \mathbf{x} are field points, ξ represent source points, while u^* and q^* represent the two well known fundamental solutions for the field variable u and its gradient, respectively [40].

After performing the spatial discretization process, the following matrix equation is obtained:

$$\mathbf{H}\mathbf{u}_{n+1} = \mathbf{G}\mathbf{q}_{n+1} - \frac{1}{c^2} \mathbf{M}\ddot{\mathbf{u}}_{n+1} \quad (7)$$

2.1. Time integration method (TIM)

The time integration methods used in this work are the proposed by Mansur in [32]. These start redefining Eq. (7) as follows:

$$(1 + \alpha)\mathbf{H}\mathbf{u}_{n+1} - \alpha\mathbf{H}\mathbf{u}_n = \mathbf{G}\mathbf{q}_{n+1} - \frac{1}{c^2} \mathbf{M}\ddot{\mathbf{u}}_{n+1} \quad (8)$$

The idea behind introducing the α parameter in Eq. (8) is to get a better control of the damping. Experience indicates that when assigning positive values to such a parameter the damping is increased and vice versa. The acceleration vector may be approximated with the Newmark [29] or the Houbolt [28] algorithms.

In the Houbolt method, the following expressions are used for time derivatives:

$$\dot{\mathbf{u}}_{n+1} = \frac{1}{6\Delta t} [11\mathbf{u}_{n+1} - 18\mathbf{u}_n + 9\mathbf{u}_{n-1} - 2\mathbf{u}_{n-2}]$$

$$\ddot{\mathbf{u}}_{n+1} = \frac{1}{\Delta t^2} [2\mathbf{u}_{n+1} - 5\mathbf{u}_n + 4\mathbf{u}_{n-1} - \mathbf{u}_{n-2}]$$

For the case when $n = 0$ the vectors \mathbf{u}_{-1} and \mathbf{u}_{-2} must be computed based on a first order Euler scheme as:

$$\mathbf{u}_{-1} = \mathbf{u}_0 - \dot{\mathbf{u}}_0 \times \Delta t$$

$$\mathbf{u}_{-2} = \mathbf{u}_0 - 2\dot{\mathbf{u}}_0 \times \Delta t$$

Besides, in the Newmark scheme, the following expressions are used for time derivatives:

$$\dot{\mathbf{u}}_{n+1} = \frac{\gamma}{\beta\Delta t^2} [\mathbf{u}_{n+1} - \mathbf{u}_n] + \frac{(\beta - \gamma)}{\beta} \dot{\mathbf{u}}_n - \frac{(\gamma - 2\beta)}{2\beta} \ddot{\mathbf{u}}_n \Delta t$$

$$\ddot{\mathbf{u}}_{n+1} = \frac{[\mathbf{u}_{n+1} - \mathbf{u}_n]}{\beta\Delta t^2} + \frac{1}{\beta\Delta t} \dot{\mathbf{u}}_n - \frac{(1 - 2\beta)}{2\beta} \ddot{\mathbf{u}}_n$$

At the beginning the accelerations in general are unknown and must be computed as:

$$\ddot{\mathbf{u}}_0 = \frac{2}{\Delta t^2} [\mathbf{u}_1 - \mathbf{u}_0 - \dot{\mathbf{u}}_0 \Delta t] \quad (9)$$

After having approximated the acceleration vector, the following generic expression is obtained:

$$\hat{\mathbf{H}}\mathbf{u}_{n+1} - \mathbf{G}\mathbf{q}_{n+1} = \mathbf{g}_n \quad (10)$$

Table 1
Definitions for generic expression.

TIM		\hat{H}	g_n
Houbolt- α	$n = 0$	$(1 + \alpha)H + \frac{2}{c^2 \Delta t^2} M$	$\alpha H u_0 + \frac{2}{c^2 \Delta t^2} M [u_0 + \dot{u}_0 \times \Delta t]$
Houbolt- α	$n > 0$	$(1 + \alpha)H + \frac{2}{c^2 \Delta t^2} M$	$\alpha H u_n - \frac{1}{c^2 \Delta t^2} M [-5u_n + 4u_{n-1} - u_{n-2}]$
Newmark- α	$n = 0$	$(1 + \alpha)H + \frac{2}{c^2 \Delta t^2} M$	$\alpha H u_0 + \frac{2}{c^2 \Delta t^2} M [u_0 + \dot{u}_0 \times \Delta t]$
Newmark- α	$n > 0$	$(1 + \alpha)H + \frac{1}{\beta c^2 \Delta t^2} M$	$\alpha H u_n + \frac{1}{\beta c^2 \Delta t^2} M [u_n + \dot{u}_n \times \Delta t + \ddot{u}_n (0.5 - \beta) \times \Delta t^2]$

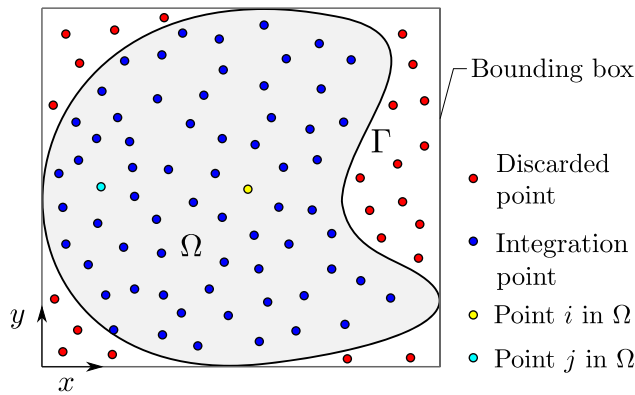


Fig. 2. Integration based on whole domain.

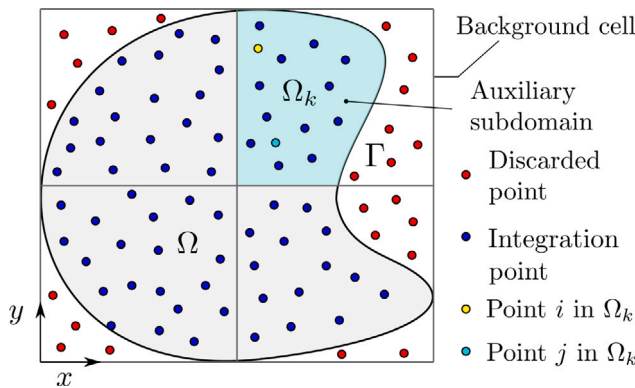


Fig. 3. Integration based on auxiliary subdomains.

Depending on the method used to approximate the acceleration the schemes may be called as Houbolt- α or Newmark- α , respectively. Some definitions for the Eq. (10) are listed in Table 1.

3. Radial basis integration method

The Radial Basis Integration Method (RBIM) uses a distributed set of points inside the whole domain or inside auxiliary sub-domains as integration points. In order to obtain greater precision it is recommended that the points be distributed in a uniform or quasi-uniform way, because the location of the singularity in the domain integrals is variable on the domain. One possible way to obtain such points is by using a bounding box and hexagonal patterns with a point at its centroid. The points outside the domain must be rejected using an appropriate algorithm (Figs. 2–3). Another alternative is to generate quasi-random distributions as in mesh-free methods [25,41].

The present method is based on our most recent work, i.e. the Kriging Integration Method [27]. The main difference is that the new approach contemplates the use of other radial basis functions different to the Gaussian but without free parameters, and they are also complemented with polynomial terms to ensure greater convergence. With the

absence of these parameters, a significant computation time saving can also be achieved with similar results. On the other hand, the evaluation of the domain integrals required to obtain the weights are now exactly converted to boundary integrals instead of being evaluated using the Cartesian Integration Method, which in general requires a significantly higher number of integration points and more specialized programming when controlling appropriate number of integration points in specific areas in quite complex domains such as those containing hundreds of arbitrary perforations of different sizes.

The theoretical foundations to get the weights of this quadrature is very similar in both methods, however, for a better understanding it is better to show it in detail as described below.

The weights of the quadrature points can be obtained by carrying out a similar procedure as in [38,42], which is based on performing certain matrix/vector operations taking into account the following augmented radial basis approximation:

$$u(\mathbf{x}) \approx \sum_{i=1}^{n_r} \alpha_i u_i + \sum_{j=1}^{n_p} \beta_j p_j(\mathbf{x}) = \Phi^T \hat{\mathbf{u}} \quad (11)$$

where n_r is the amount of points employed with the RBF, n_p refer to the number of polynomial terms, u_i are the values of the variable to be approximated, $\Phi = [\alpha_1, \alpha_2, \dots, \alpha_{n_r}, \beta_1, \beta_2, \dots, \beta_{n_p}]^T$ where α and β are unknown coefficients, while

$$\hat{\mathbf{u}} = [u_1, u_2, u_3, \dots, u_{n_r}, 0, 0, 0, \dots, 0]^T \text{ whose size is } (n_r + n_p) \times 1. \text{ The vector } \Phi \text{ can be obtained as follows:}$$

$$\Phi = A^{-1} \mathbf{v} = \begin{bmatrix} C & P^T \\ P & \mathbf{0} \end{bmatrix}^{-1} \begin{bmatrix} \mathbf{v}_r \\ \mathbf{v}_p \end{bmatrix} \quad (12)$$

where the elements of matrix C are defined by $C_{ij} = C(\mathbf{x}_i, \mathbf{x}_j) = f(r_{ij})$ in which f is a function that belongs to a group of RBFs evaluated for each point combination i and j (See Fig. 2).

$\mathbf{v}_r = [C(\mathbf{x}_1, \mathbf{x}), C(\mathbf{x}_2, \mathbf{x}), \dots, C(\mathbf{x}_{n_r}, \mathbf{x})]^T$, $\mathbf{v}_p = \mathbf{v}_p(\mathbf{x}) = [1, p_1(\mathbf{x}), p_2(\mathbf{x}), \dots, p_{n_p}(\mathbf{x})]^T$ and the matrix P may be defined in compact form as follows:

$$P = [\mathbf{v}_p(\mathbf{x}_1), \mathbf{v}_p(\mathbf{x}_2), \dots, \mathbf{v}_p(\mathbf{x}_{n_r})]_{n_p \times n_r}$$

The required weights could be computed for the whole domain or alternatively for auxiliary sub-domains. The integral of function $u(\mathbf{x})$ over the k th auxiliary sub-domain using the present method may be computed as follows:

$$\int_{\Omega_k} u(\mathbf{x}) d\Omega_k = \int_{\Omega_k} \Phi^T \hat{\mathbf{u}} d\Omega_k = \int_{\Omega_k} (A_k^{-1} \mathbf{v})^T \hat{\mathbf{u}} d\Omega_k \quad (13)$$

with the matrix A_k^{-1} defined as in Eq. (12) for the k th sub-domain. However, the integral defined above can also be calculated according to the following quadrature:

$$\int_{\Omega_k} u(\mathbf{x}) d\Omega \approx \langle \mathbf{w}_k, \hat{\mathbf{u}} \rangle = \langle \mathbf{w}_k, \mathbf{u} \rangle = \sum_{i=1}^{n_r} w_i^k u_i \quad (14)$$

Therefore, it is inferred that

$$\mathbf{w}_{\Omega_k} = \int_{\Omega_k} (A_k^{-1} \mathbf{v}) d\Omega_k = A_k^{-1} \int_{\Omega_k} \mathbf{v} d\Omega_k \quad (15)$$

or

$$\begin{bmatrix} \mathbf{w}_k \\ \mathbf{z}_k \end{bmatrix} = \begin{bmatrix} C_k & (P_k)^T \\ P_k & \mathbf{0} \end{bmatrix}^{-1} \int_{\Omega_k} \begin{bmatrix} \mathbf{v}_r \\ \mathbf{v}_p \end{bmatrix} d\Omega_k$$

The domain integrals that appear in the Eq. (15) may be converted into the boundary by using the Green Theorem. Therefore,

$$\int_{\Omega_k} C_k(\mathbf{x}_n, \mathbf{x}) d\Omega_k = \int_{\Gamma_k} \left(\int_a^x C_k(\mathbf{x}_n, \mathbf{x}) dx \right) n_x d\Gamma_k \tag{16}$$

$$= \int_{\Gamma_k} D_k(\mathbf{x}_n, \mathbf{x}) n_x d\Gamma_k$$

$$\int_{\Omega_k} P_k^i(\mathbf{x}) d\Omega_k = \int_{\Gamma_k} \left(\int_a^x P_k^i(\mathbf{x}) dx \right) n_x d\Gamma_k \tag{17}$$

$$= \int_{\Gamma_k} E_k^i(\mathbf{x}) n_x d\Gamma_k$$

where a is an arbitrary constant. As indicated in [26], only when the interior integral is evaluated numerically is it necessary to set the value of a as follows:

$$a = \frac{\sum_{j=1}^m x_j}{m}$$

where x_j is the abscissa of the j th node of the discretized boundary using m boundary element nodes.

Thus, the discretized form of Eqs. (16) and (17) are given by:

$$\int_{\Omega_k} C_k(\mathbf{x}_n, \mathbf{x}) d\Omega_k = \sum_{e=1}^{l_k} \int_{\Gamma_k^e} D_k(\mathbf{x}_n, \mathbf{x}) dy \tag{18}$$

$$= \sum_{e=1}^{l_k} \int_{-1}^{+1} D^k(\mathbf{x}_n, \mathbf{x}(\xi)) \left(\frac{dy(\xi)}{d\xi} \right) d\xi$$

$$\int_{\Omega_k} P_k^i(\mathbf{x}) d\Omega_k = \sum_{e=1}^{l_k} \int_{\Gamma_k^e} E_k^i(\mathbf{x}) dy \tag{19}$$

$$= \sum_{e=1}^{l_k} \int_{-1}^{+1} E_i^k(\mathbf{x}(\xi)) \left(\frac{dy(\xi)}{d\xi} \right) d\xi$$

with $x(\xi) = \sum_{j=1}^m \phi_j x_j^e$, $y(\xi) = \sum_{j=1}^m \phi_j y_j^e$ and $\frac{dy(\xi)}{d\xi} = \sum_{j=1}^m \frac{d\phi_j}{d\xi} y_j^e$, in which ϕ_j are shape functions.

Among the functions that we have been tested to get the weights of the present method are :

- The Gaussian $f_j = e^{-c(\frac{r_j}{r_{max}})^2}$, with the parameters c and r_{max} defined as in [43].
- The thin plate spline $f_j = r_j^2 \ln(r_j)$, which it was recommended in [44]. It can also be expressed as $f_j = r_j \ln(r_j^r)$ to avoid numerical problems at $r_j = 0$.
- The polyharmonic spline $f_j = r_j^4 \ln(r_j)$, which can also be expressed as $f_j = r_j^3 \ln(r_j^r)$ to avoid numerical problems at $r_j = 0$.

where subscript j indicates that the function is centered at point j .

Actually the problem of evaluating the last two functions when r_j tends to zero occurs only when the direct substitution $r_j = 0$ is made, however, $\lim_{r_j \rightarrow 0} (r_j^4 \ln(r_j)) = 0$, so for this case $f_j = 0$. If the suggested equivalent expression $f_j = r_j^3 \ln(r_j^r)$ is not used, alternatively a very small value such as $\epsilon = 2.2204 \times 10^{-16}$ can be added to the logarithmic term, i.e. $f_j = r_j^4 \ln(r_j + \epsilon)$ and the same value given by the limit would be obtained.

It should be noted that in the present method the functions used to calculate the weights of any distribution of points as part of a quadrature that estimates the value of the integral of an unknown function must have the property of being interpolant (which possesses the Kronecker delta property) since such weights are associated with the values for which both functions coincide when evaluated at those locations. The RBFs that are good candidates to get the best integration weights are those for which the inverse of the interpolating matrix A_k can be calculated without inconvenience, that is, those that have a relatively low condition number compared to the number of points used. It is also important that such radial basis functions have adequate local behavior

that guarantees convergence. In this sense, positive-defined compact radial basis functions, including those based on semivariograms such as the Gaussian and also conditionally positive-defined functions such as the Thin Plate Spline (TPS) and the Polyharmonic Spline augmented with polynomial terms, may be suitable for obtaining the weights.

On the other hand, to approximate the source term in the RBI-BEM formulation, both interpolant or approximant meshless functions could be used. If the source term has a known mathematical expression or some values are known at some points (not necessarily at the poles), then approximant functions such as the based on Moving Least Squares (MLS), or any radial basis interpolant function can be used. However, sometimes the source term is a function of the unknown variable of the problem and even its derivatives and the meshless functions must pass through the values of the unknown function at such collocation points, and it is also required to impose boundary conditions, so in this particular case they must be interpolant. In this sense, taking into account that the radial basis functions can be used in both situations and their derivatives are easier to calculate, they were chosen in this work to approximate the source term as is done in DR-BEM. Unlike the radial basis functions used to calculate the quadrature weights, the functions used to approximate the source term do not necessarily have to be positive-defined or with compact support.

In this work we used the Polyharmonic Spline $f_j = r_j^3 \ln(r_j^r)$ supplemented with the monomial family $\{1, x, y\}$ because with this, lower error percentages were obtained against integration obtained analytically or by other methods than when using the Thin Plate Spline in some tests. For the Polyharmonic Spline the antiderivative $D_k(\mathbf{x}_n, \mathbf{x})$ can be integrated analytically after performing the variable changes $\tilde{x} = x - x_n$ and $\tilde{y} = y - y_n$. We can choose for convenience $a = x_n$ in order to get a shorter expression, so the new integration limits become 0 and \tilde{x} . Such integral was calculated with the symbolic algebra program Wx-Maxima, obtaining the following simplified expression:

$$D_k(\mathbf{x}_n, \mathbf{x}) = \frac{(225\tilde{x}\tilde{y}^4 + 150\tilde{x}^3\tilde{y}^2 + 45\tilde{x}^5) \ln(\tilde{y}^2 + \tilde{x}^2)}{450} + \frac{240\tilde{y}^5 \arctan(\tilde{x}/\tilde{y}) - 240\tilde{x}\tilde{y}^4 - 70\tilde{x}^3\tilde{y}^2 - 18\tilde{x}^5}{450}$$

On the other hand, each monomial could be transformed to the boundary using a different value of a because the integration is calculated analytically and therefore its value can be arbitrary. With the idea of getting the shortest expression of the integrand, $a = 0$ was chosen for such integrals, so we got the following terms:

$$E_k^1(\mathbf{x}) = x, \quad E_k^2(\mathbf{x}) = \frac{x^2}{2}, \quad E_k^3(\mathbf{x}) = xy$$

Then, using the previous expressions, the integrals in Eqs. (18) and (19) can be calculated numerically to obtain the integration weights from the matrix definition of Eq. (15).

All singular domain integrals present in boundary elements can be expressed in discretized form as follows:

$$I_i = \int_{\Omega} b(\mathbf{x}) u^*(\xi^i, \mathbf{x}) d\Omega \equiv \sum_{k=1}^{NS} \int_{\Omega_k} b(\mathbf{x}) u^*(\xi^i, \mathbf{x}) d\Omega_k \tag{20}$$

where $i = 1, 2, \dots, M$. Here $b(\mathbf{x})$, u^* , \mathbf{x} and ξ^i stand for the source term, the fundamental solution, the field points and source points, respectively. The source term may be approximated as in the Dual reciprocity method as follows:

$$b(\mathbf{x}) = \sum_{j=1}^m \alpha_j f_j(\mathbf{x}) = \mathbf{f}^T(\mathbf{x}) \boldsymbol{\alpha} \tag{21}$$

where m represent the sum of boundary and domain nodes, f_j are the RBFs for each application point and α_j are unknown coefficients. In vector notation the following definition are given:

$$\mathbf{f}^T(\mathbf{x}) = [f_1(\mathbf{x}), f_2(\mathbf{x}), \dots, f_m(\mathbf{x})] \text{ and } \boldsymbol{\alpha} = \mathbf{F}^{-1} \mathbf{b} \text{ where } \mathbf{F} = [f(\mathbf{x}^1), f(\mathbf{x}^2), \dots, f(\mathbf{x}^m)]. \text{ Therefore, Eq. (20) can be rewritten as:}$$

$$I_i = \sum_{k=1}^{NS} \int_{\Omega_k} u^*(\xi^i, \mathbf{x}) \mathbf{f}^T(\mathbf{x}) d\Omega_k \mathbf{F}^{-1} \mathbf{b}$$

Applying the present method we have:

$$I_i = [S_{i1}, S_{i2}, \dots, S_{ij}, \dots, S_{im}] F^{-1} b$$

where

$$S_{ij} = \sum_{k=1}^{NS} \int_{\Omega_k} f_j(\mathbf{x}) u^*(\xi^i, \mathbf{x}) d\Omega_k \approx \sum_{k=1}^{NS} \mathbf{w}_k^T f_j(\mathbf{Q}_k) \bullet u^*(\xi^i, \mathbf{Q}_k) \equiv \sum_{k=1}^{NS} \mathbf{w}_k^T \mathbf{h}_j(\xi^i, \mathbf{Q}_k) \quad (22)$$

Here \mathbf{w}_k refer to the vector of the integration weights and the symbol \bullet represents an element-wise product. The vector \mathbf{h}_j contains the function values for each quadrature point inside the k th subdomain. Unlike RI-BEM in RBI-BEM by applying Green's theorem the inner integral is computed with respect to the abscissa coordinate, therefore R_j it is not necessary to be defined as a function of r_i (Fig. 1). In Eq. (22) only if $\mathbf{Q}_k^m \neq \xi^i$ there is a contribution to the integral, being \mathbf{Q}_k^m the m th integration point in the k th subdomain.

The column vector of domain integrals may be expressed in compact way as follows:

$$I = S F^{-1} b \quad (23)$$

where

$$S = \begin{bmatrix} S_{11} & S_{12} & \dots & S_{1m} \\ S_{21} & S_{22} & \dots & S_{2m} \\ \vdots & \vdots & \ddots & \vdots \\ S_{m1} & S_{m2} & \dots & S_{mm} \end{bmatrix}$$

Following a similar procedure for the approximation of $\ddot{u}(t)$ in the scalar wave equation we have:

$$I = S F^{-1} \ddot{u} = M \ddot{u} \quad (24)$$

It must be highlighted that if the domain is partitioned into subdomains we get the following advantages:

- The size of matrix A^{-1} is reduced, thus, the calculation of the weights is done more quickly.
- Different types of singularities could be treated by only applying MRI-BEM or LIM over the auxiliary subdomains that represent the near field of the singular point.
- It could be possible to accelerate RBI-BEM with ACA or Fast Multipole Methods (FMMs).

3.1. Weakly singular domain integrals

In RBI-BEM, in the same way as in the Cartesian Integration Method (CTM) [26] and the combined approach called DIBEM-RIM [37], regularization techniques can be used to treat weakly singular integrals, however, experience has shown that the results obtained using regularization can be even less precise than the achieved by the untreated ones. Additionally, it was inferred from the mathematical development carried out in [27] that the presence of logarithmic singularities does not significantly affect the direct evaluation of domain integrals, therefore, in this work these integrals are calculated using a quadrature obtained from the Radial Basis Integration Method and discarding the possible integration point where the radial distance between this and the source point becomes zero.

4. Review of the modified radial integration method

This is a modified version of the radial integration method. It was specially developed to convert domain integrals into boundary ones over non-convex domains. In general, the source term that appears in domain integrals is approximated by RBFs, therefore, these integrals are defined as follows:

$$I_i = \int_{\Omega} b(\mathbf{x}) u^*(\xi^i, \mathbf{x}) d\Omega = \sum_{j=1}^m \gamma_j I_j(\xi^i) \quad (25)$$

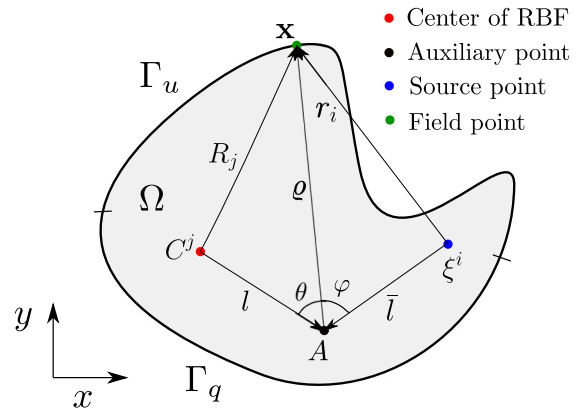


Fig. 4. Physical domain and relationship among variables.

where $I_j(\xi^i) = \int_{\Omega} \phi_j(R_j) u^*(\xi^i, \mathbf{x}) d\Omega$, which is transformed by using the Modified Radial Integration Method to the following equivalent boundary integral [45]:

$$I_j(\xi^i) = \int_{\Gamma} \frac{\partial \rho}{\partial n} \frac{F_j(\xi^i)}{\rho} d\Gamma(\mathbf{x}) \quad (26)$$

in which

$$F_j(\xi^i) = \int_0^{\rho} \phi_j(R_j) u^*(r_i) \rho d\rho \quad (27)$$

The distances r_i and R_j are expressed as function of the new variable ρ from an auxiliary point as shown in Fig. 4. These distances are calculated as follows:

$$r_i = \sqrt{\rho^2 + \bar{l}^2 - 2\rho\bar{l}\cos(\varphi)} \quad (28)$$

$$R_j = \sqrt{\rho^2 + l^2 - 2\rho l \cos(\theta)} \quad (29)$$

The right side of Eq. (25) may alternatively be written in matrix notation as:

$$I_i = [I_1(\xi^i), I_2(\xi^i), \dots, I_m(\xi^i)] F^{-1} \begin{bmatrix} b_B \\ b_D \end{bmatrix}$$

5. Implementation

There are several possibilities to implement the present method, among them we have:

5.1. Subroutine 1

- 1: Discretize the boundary of the whole domain.
- 2: Generate points inside a bounding box that circumscribes the domain, then search and store the N_p integration points inside the domain. Alternatively, any algorithm/software as in meshfree methods to get the points may be used.
- 3: **if** $N_p > 2$ **then**
- 4: Perform the Radial Basis Integration Method
- 5: Store the respective coordinates and their weights in a list to be used in the RBI-BEM formulation.
- 6: **end if**

5.2. Subroutine 2

- 1: Perform a partition of the domain into auxiliary sub-domains by intercepting background cells with the domain and discretizes its boundaries.

- 2: Generate integration points inside a bounding box that circumscribes the whole domain.
- 3: **for** $i \leftarrow 1, N_S$ **do**
- 4: Search and store the N_p integration points inside the i th sub-domain.
- 5: **if** $N_p > 2$ **then**
- 6: Perform the Radial Basis Integration Method in the i th auxiliary sub-domain.
- 7: Store the respective coordinates and their weights in a multi-dimensional list to be used in the RBI-BEM formulation.
- 8: **end if**
- 9: **end for**

5.3. Subroutine 3

- 1: Perform a partition of the domain into auxiliary sub-domains by intercepting background cells with the domain and discretizes its boundaries.
- 2: **for** $i \leftarrow 1, N_S$ **do**
- 3: Generate the integration points inside the i th subdomain using any algorithm/software as in mesh free methods.
- 4: Perform the Radial Basis Integration Method in the i th auxiliary sub-domain.
- 5: Store the respective coordinates and their weights in a multi-dimensional list to be used in the RBI-BEM formulation.
- 6: **end for**

5.4. Subroutine 4

- 1: Perform a partition of the domain by using a Centroidal Voronoi Tessellation
- 2: **for** $i \leftarrow 1, N_S$ **do**
- 3: Generate the integration points inside the i th subdomain using any algorithm/software as in mesh free methods.
- 4: Perform the Radial Basis Integration Method in the i th auxiliary sub-domain.
- 5: Store the respective coordinates and their weights in a multi-dimensional list to be used in the RBI-BEM formulation.
- 6: **end for**

It is important to highlight that the quadrature is generated offline and used by the main code similarly as with any standard quadrature.

6. Numerical examples

In the present work four examples were selected from some benchmark problems. For the generation of the integration quadrature with the Radial Basis Integration Method, subroutine 1 was consider because the examples addressed here do not belong to the category of large-scale problems and relatively few elements and internal points were used. In order to get better results in the MRI-BEM four and six integration points were used for boundary and radial integrals respectively. Although other types of radial basis functions could be compared, only the well known linear and cubic RBFs, were tested in several examples using both domain and boundary nodes for its construction. The singular boundary integrals were computed with the usual rigid body motion approach.

Here as in [26,27] the ratio $\mathfrak{R} = d/d_{int}$ was used as a measure of the appropriate quantity of Radial Basis Integration points. Where the numerator represent the mean distance among all internal points, while the denominator is the mean distance of the Radial Basis Integration points.

The average relative error e_r between the present method and others solutions, taking into account all time steps within the used time interval is computed based on the norm L_2 .

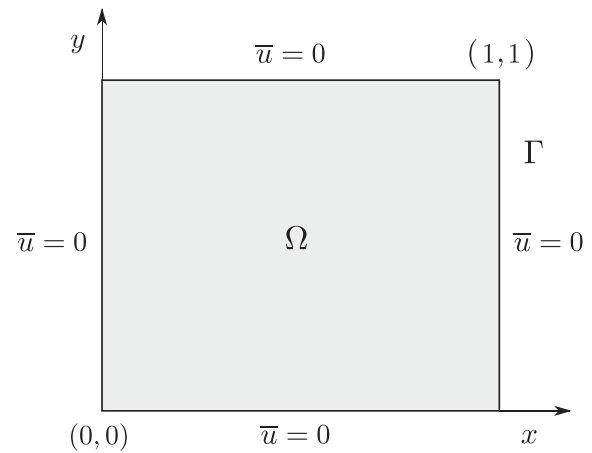


Fig. 5. Square domain.

Table 2 Results at point A for example 1.

Approach	f_j	Houbolt- α		Newmark- α	
		e_r	t(s)	e_r	t(s)
DR-BEM	$1 + r_j$	0.043	7.88	0.044	9.27
RBI-BEM		0.057	9.57	0.054	9.64
MRI-BEM		0.081	845	0.059	812

In Tables 2–5 the term $t(s)$ stand for the execution time in seconds of the respective BEM approaches codes.

For comparison purposes, we tried to maintain the same parameters and Δt for the same time marching method in the different BEM approaches, however, due to the instability in some methods some modifications were necessary. Which is discussed at the end of the paper.

6.1. Example 1

A unitary square region representing a clamped membrane with the below prescribed initial conditions is considered (Fig. 5).

$$u(x, y, 0) = x(x - 1)y(y - 1) \quad (x, y) \in \Omega \tag{30}$$

$$\dot{u}(x, y, 0) = 0 \quad (x, y) \in \Omega \tag{31}$$

The respective theoretical solution may be found in [3]. Here the wave propagation velocity was taken as 1 m/s. The variation of u at membrane's center was gotten using 80 constant boundary elements and 81 domain points in combination with Houbolt- α and Newmark- α for a normalized time inside the interval $[0, 5]$. For the present method the integration points were generated using the NodeLab Matlab's package considering $\mathfrak{R} = 1.98$. Comparison of potential obtained from the present method, DR-BEM, MRI-BEM and the theoretical solution using the linear function $f_j = 1 + r_j$ are provided in Figs. 6–7, in which the results for all compared methods are shown to be in close agreement with the obtained theoretically. According to Table 2, DR-BEM was slightly more accurate than RBI-BEM, while that with MRI-BEM the less approximate solution was obtained. The achieved results for RBI-BEM and MRI-BEM with the Newmark- α method were better than with the Houbolt- α method, however for both time marching schemes used with DR-BEM the solutions were practically the same. Additionally, no significant difference is observed in the execution times between DR-BEM and RBI-BEM, but the same cannot be said for the difference between these two and MRI-BEM.

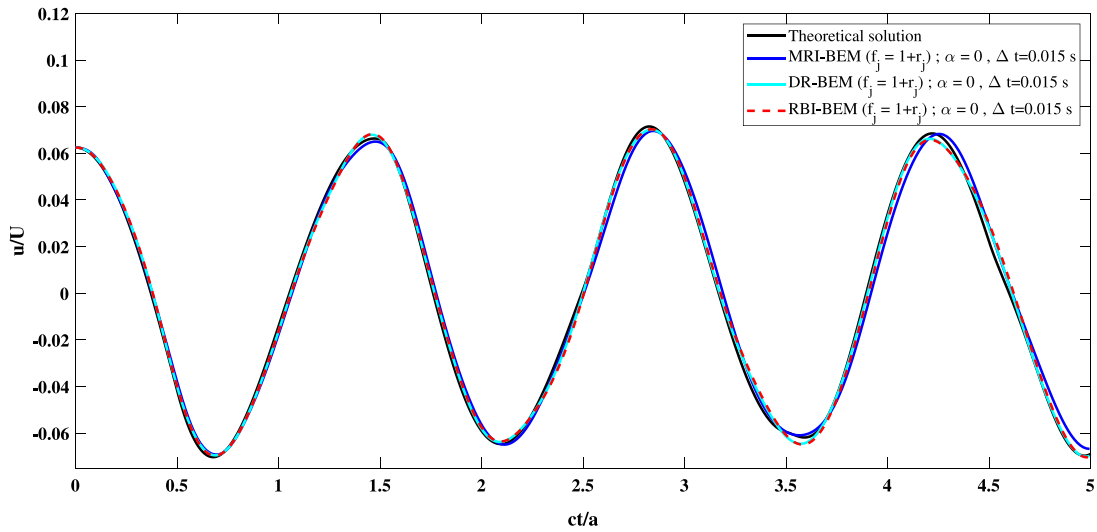


Fig. 6. Displacement at point (0.5, 0.5) with Houbolt- α method.

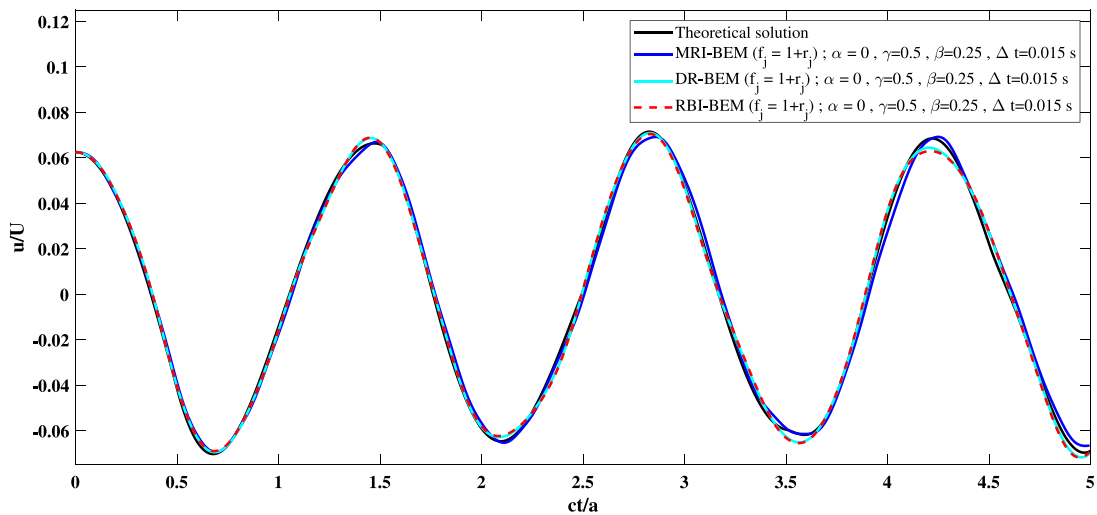


Fig. 7. Displacement at point (0.5, 0.5) with Newmark- α method.

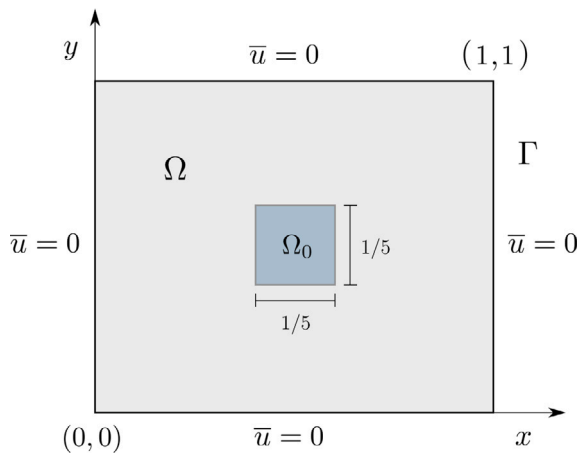


Fig. 8. Square domain.

Table 3
Results at point A for example 2.

Approach	f_j	Houbolt- α		Newmark- α	
		e_r	t(s)	e_r	t(s)
DR-BEM		0.110	26.86	0.132	10.33
RBI-BEM	$1 + r_j$	0.108	112.42	0.116	156.3
MRI-BEM		0.84	25995.3	0.854	28594
DR-BEM		0.804	27.07	0.88	13.16
RBI-BEM	r_j^3	0.214	294.27	0.14	273.3
MRI-BEM		0.932	15640	0.94	21788

6.2. Example 2

Here as in the before example both the same geometry with clamped sides and propagation wave velocity were considered but in this case under others initial conditions which are given as (Fig. 8):

$$u(x, y, 0) = 0 \quad (x, y) \in \Omega \tag{32}$$

$$\dot{u}(x, y, 0) = V_0 = 1 \quad (x, y) \in \Omega_0 \tag{33}$$

where Ω_0 belongs to the domain center. The analytical solution is shown in [2].

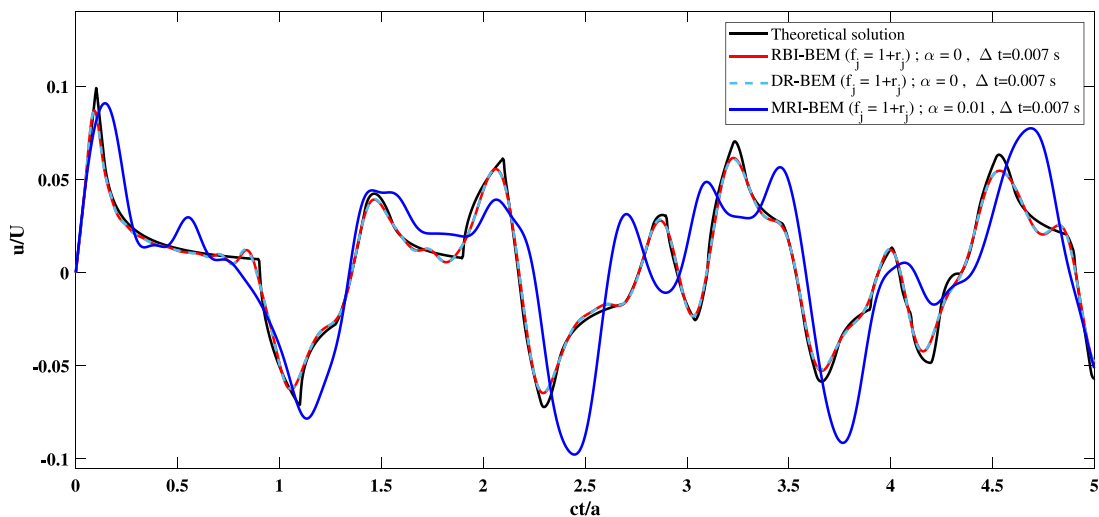


Fig. 9. Displacement at point (0.5, 0.5) with $f_j = 1 + r_j$ and Houbolt- α method.

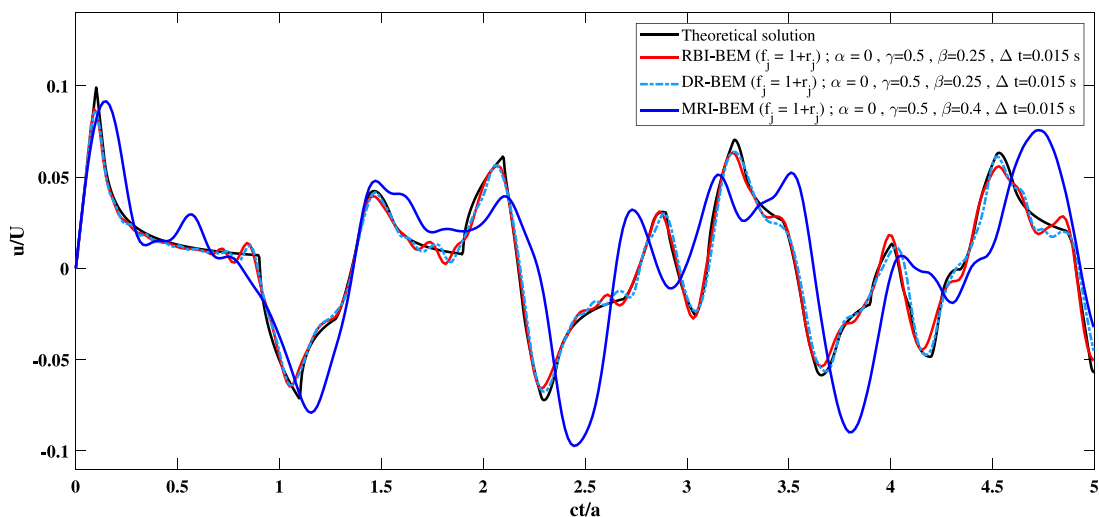


Fig. 10. Displacement at point (0.5, 0.5) with $f_j = 1 + r_j$ and Newmark- α method.

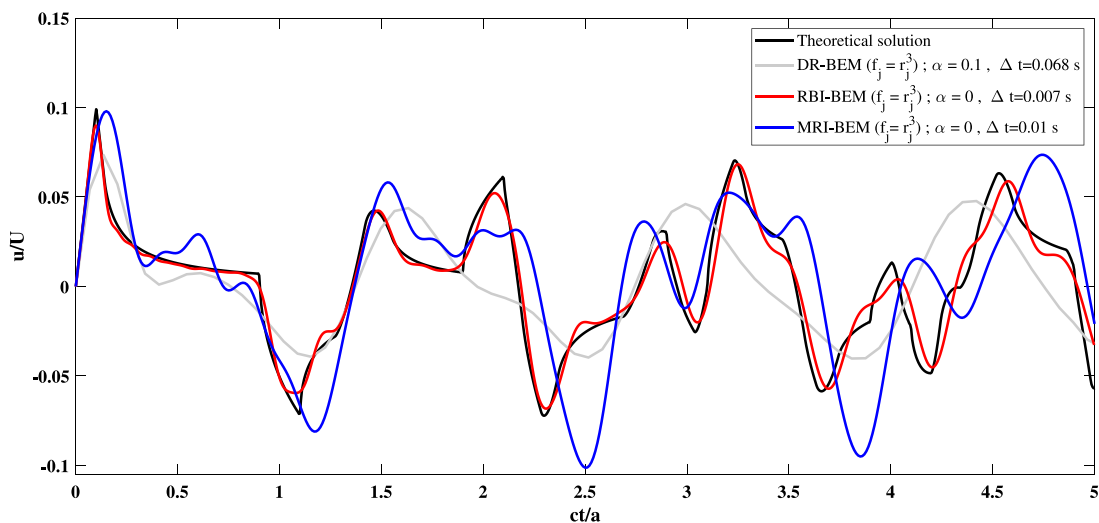


Fig. 11. Displacement at point (0.5, 0.5) with $f_j = r_j^3$ and Houbolt- α method.

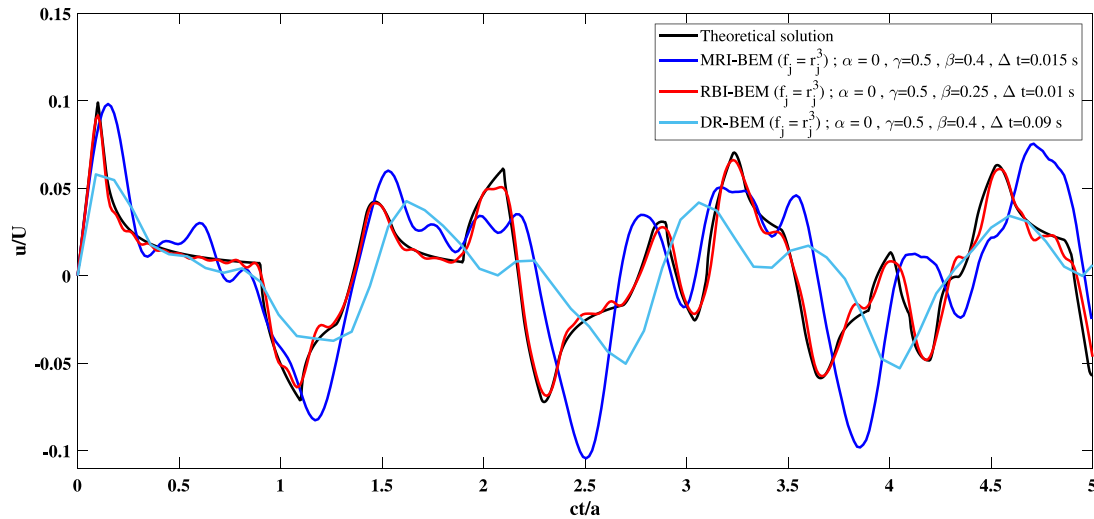


Fig. 12. Displacement at point (0.5, 0.5) with $f_j = r_j^3$ and Newmark- α method.

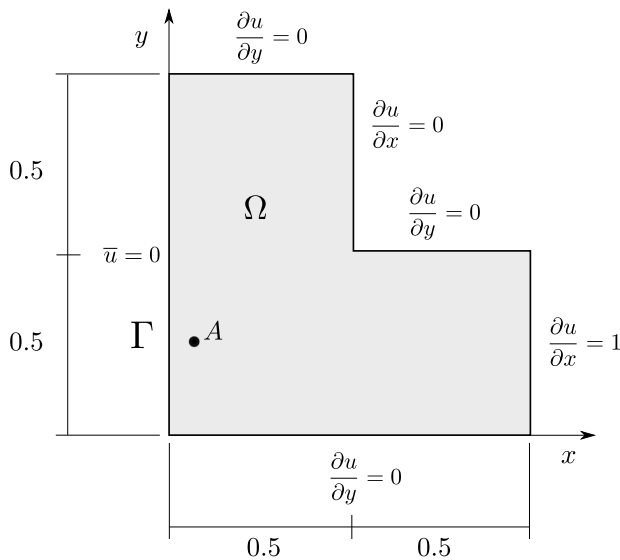


Fig. 13. Geometry and boundary condition data for example 3.

For this problem the initial non-zero velocity conditions were imposed directly on the poles belonging to Ω_0 . The variation of u at the center of membrane was obtained using 80 constant boundary elements plus 625 domain nodes. This problem was solved with CIM in [2] and using a mesh that almost triples the amount of nodes used here, however, this nodal discretization becomes relatively prohibitive for MRI-BEM due to the high computation time required to calculate the integrals. For the present method the integration points were generated using the NodeLab Matlab’s package for which the ratio $\mathfrak{R} = 1.92$ was obtained. The displacement solution at the center of membrane was obtained using Houbolt- α and Newmark- α methods. Comparison of potential obtained from the present method, DR-BEM, MRI-BEM and the theoretical solution are provided in Figs. 9–10 and Figs. 11–12 respectively. The results showed for DR-BEM and RBI-BEM in Fig. 9–10 are very similar to those obtained by the theoretical solution. However, as shown in Figs. 11–12 bad results were obtained when using $f_j = r_j^3$ in DR-BEM which is related to instability and convergence problems. It is evident in Table 3 that RBI-BEM is the most accurate of all. DR-BEM was slightly less accurate than RBI-BEM for $f_j = 1 + r_j$ using both time marching schemes, while the performance of MRI-BEM was very

Table 4
Results at point A for example 3.

Approach	f_j	Houbolt- α		Newmark- α	
		e_r	t(s)	e_r	t(s)
DR-BEM	$1 + r_j$	0.47	2.34	0.359	3.25
RBI-BEM		0.273	6.48	0.309	8.23
MRI-BEM		0.217	390	0.215	192
DR-BEM	r_j^3	0.82	2.39	0.785	2.62
RBI-BEM		0.153	6.48	0.167	8.27
MRI-BEM		0.237	393.4	0.287	298.35

unsatisfactory in all cases, since a high level of average relative error in the results and a very high execution time were achieved.

6.3. Example 3

In this example a concave L-shaped domain under mixed boundary conditions is considered (Fig. 13). Here $c=1$ m/s was adopted.

In this problem we used 56 constant boundary elements plus 50 domain nodes. It was also solved by MRI-BEM in [34] using a similar discretization. The solution for u at point A(0.05, 0.25) in the interval $0 < t \leq 15$ s was obtained using the Newmark- α and the Houbolt- α methods. Comparisons among present method, DR-BEM, MRI-BEM and Comsol using a relative fine mesh are provided in Figs. 14–17. In which it is possible to see that only the curves of RBI-BEM and MRI-BEM are in close agreement with those obtained by Comsol.

From Table 4 it is possible to make the following inferences:

- MRI-BEM performed better than RBI-BEM when using $f_j = 1 + r_j$.
- In RBI-BEM the standard Houbolt ($\alpha = 0$) and the standard Newmark ($\alpha = 0$) without numerical damping ($\gamma = 1/2, \beta = 1/4$) were used, while that combining MRI-BEM with $f_j = r_j^3$ and the Newmark- α different parameters had to be set in order to get stability and accuracy.
- The performance of RBI-BEM was notably superior to the MRI-BEM when $f_j = r_j^3$ was employed.
- The performance of DR-BEM was unsatisfactory in all tested cases.

6.4. Example 4

Here a domain with a more complicated geometry whose boundary is clamped was selected taking as reference the problem analyzed

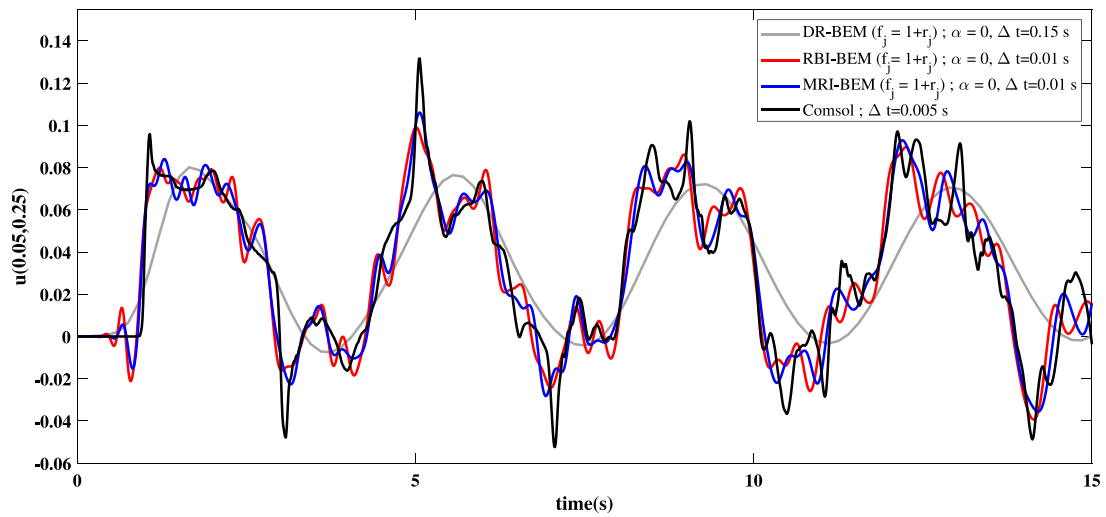


Fig. 14. L-shaped domain under mixed boundary condition: Potential at point $A(0.05, 0.25)$ with $f_j = 1 + r_j$ and the Houbolt- α method.

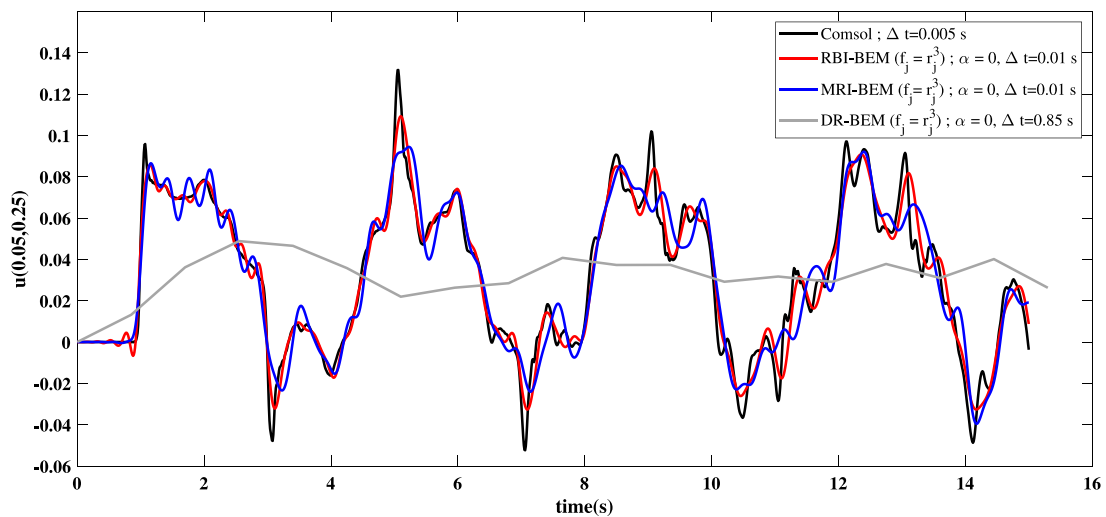


Fig. 15. L-shaped domain under mixed boundary condition: Potential at point $A(0.05, 0.25)$ with $f_j = r_j^3$ and the Houbolt- α method.

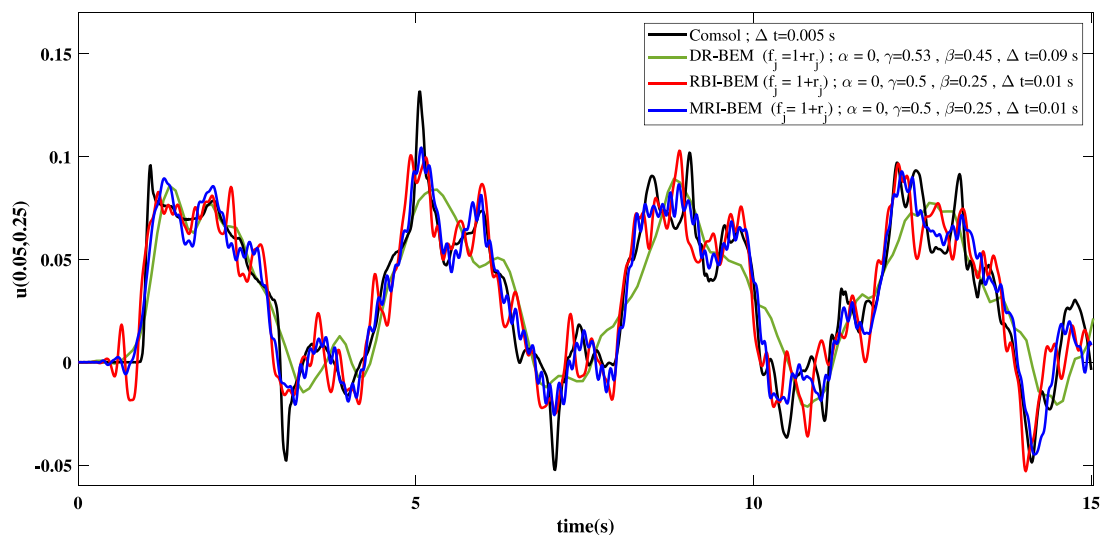


Fig. 16. L-shaped domain under mixed boundary condition: Potential at point $A(0.05, 0.25)$ with $f_j = 1 + r_j$ and the Newmark- α method.

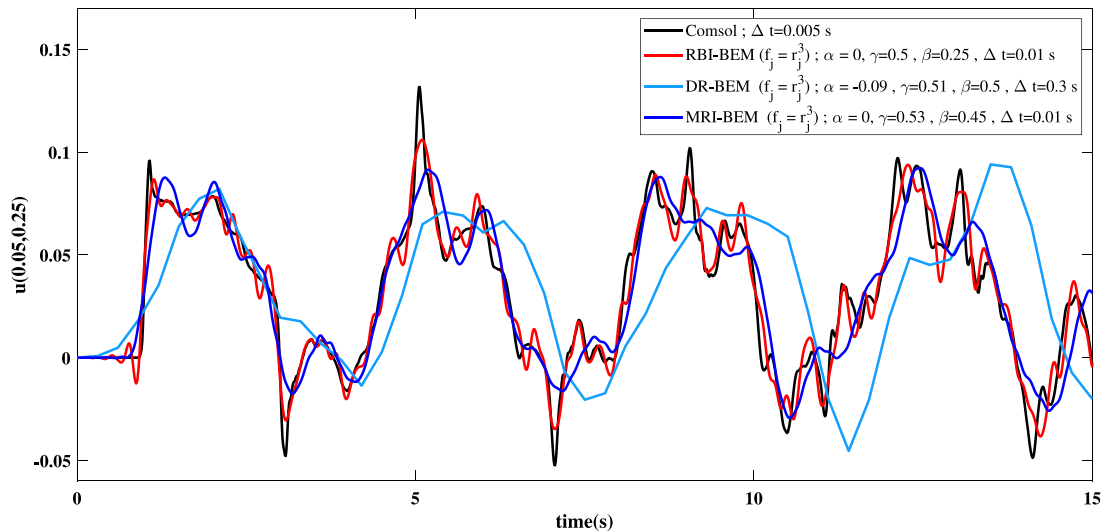


Fig. 17. L-shaped domain under mixed boundary condition: Potential at point $A(0.05, 0.25)$ with $f_j = r_j^3$ and the Newmark- α method.

Table 5
Results at point A for example 4.

Approach	f_j	Houbolt- α		Newmark- α	
		e_r	t(s)	e_r	t(s)
DR-BEM		0.655	43.5	0.788	10.31
RBI-BEM	$1 + r_j$	0.625	61.7	0.753	45.12
MRI-BEM		0.537	6275.87	0.593	9720
DR-BEM		0.97	9.21	1.03	13.61
RBI-BEM	r_j^3	0.245	121.2	0.252	104.65
MRI-BEM		0.702	6851	0.738	4888

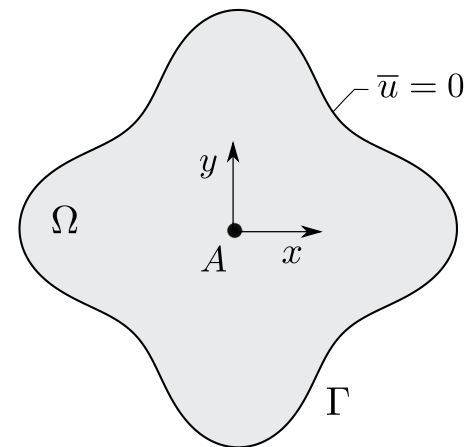


Fig. 18. Irregular shape with a parametric based boundary.

in [46] (Fig. 18). The closed region Ω is bounded by the parametric curve:

$$x = r_0 \cos \theta, \quad y = r_0 \sin \theta, \quad \theta \in [0, 2\pi) \tag{34}$$

where r_0 is defined as:

$$r_0 = \left[\cos(4\theta) + \sqrt{3.6 - \sin^2(4\theta)} \right]^{1/3} \tag{35}$$

The initial values are defined using the following expressions:

$$u(x, y, 0) = \frac{e^{-0.16(x^2+y^2)}}{10} \quad (x, y) \in \Omega \tag{36}$$

$$\dot{u}(x, y, 0) = 0 \quad (x, y) \in \Omega \tag{37}$$

The variation of u at the center of membrane was obtained using 60 constant boundary elements plus 405 domain nodes. A similar scaled problem using 60 boundary points and 1205 interior nodes was analyzed employing a Meshless approach in [46], however, for comparison purposes, only 405 internal nodes were used in our analysis, taking into account that MRI-BEM requires high computation time. The NodeLab Matlab's package was used in the present method for the generation of integration points setting a ratio $\mathfrak{R} = 2$. As in the previous examples the same time marching stepping schemes were used. Due to the analytical solution is unavailable, all the BEM approaches were compared with results obtained with Comsol, using 17092 triangular quadratics elements and 34483 nodal points. Results are depicted in Figs. 19–22.

From Table 5 it is possible to make the following inferences:

- MRI-BEM performed better than RBI-BEM for $f_j = 1 + r_j$ using both time marching schemes.
- The performance of RBI-BEM was notably superior to the MRI-BEM when $f_j = r_j^3$ was employed, although with the standard

Table 6
Minimum time step required for stability for all examples using Houbolt- α .

f_j	Example	Approach		
		DR-BEM	MRI-BEM	RBI-BEM
$1 + r_j$	1	0.0005 s	0.0005 s	0.0005 s
	2	0.0005 s	0.001 s	0.0005 s
	3	0.15 s	0.0005 s	0.0005 s
	4	0.07 s	0.01 s	0.2 s
r_j^3	1	0.0005 s	0.0005 s	0.0005 s
	2	0.07 s	0.01 s	0.0005 s
	3	0.85 s	0.0005 s	0.0005 s
	4	1.0	0.03 s	0.007 s

Newmark method ($\alpha = 0$), the parameters $\gamma = 0.53$ and $\beta = 0.3$ had to be set in order to get more accuracy .

- The performance of DR-BEM was unsatisfactory in all tested cases, and several set of parameters had to be set with the standard Newmark ($\alpha = 0$) in order to achieve stability and better results.
- MRI-BEM is very time consuming compared with DR-BEM and RBI-BEM.

It can be highlighted that the present method achieved a similar accuracy than Comsol using only few collocation points.

Although it seems unfair to compare several cases of the different approaches under different time steps, the reasons are actually due

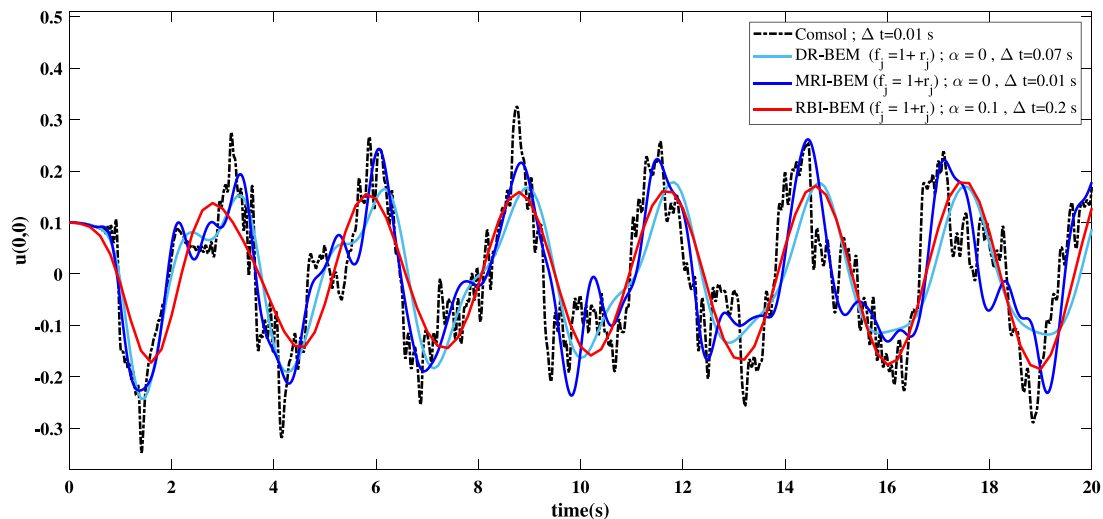


Fig. 19. Irregular domain with a smooth edge: Potential at point $A(0,0)$ with $f_j = 1 + r_j$ and the Houbolt- α method.

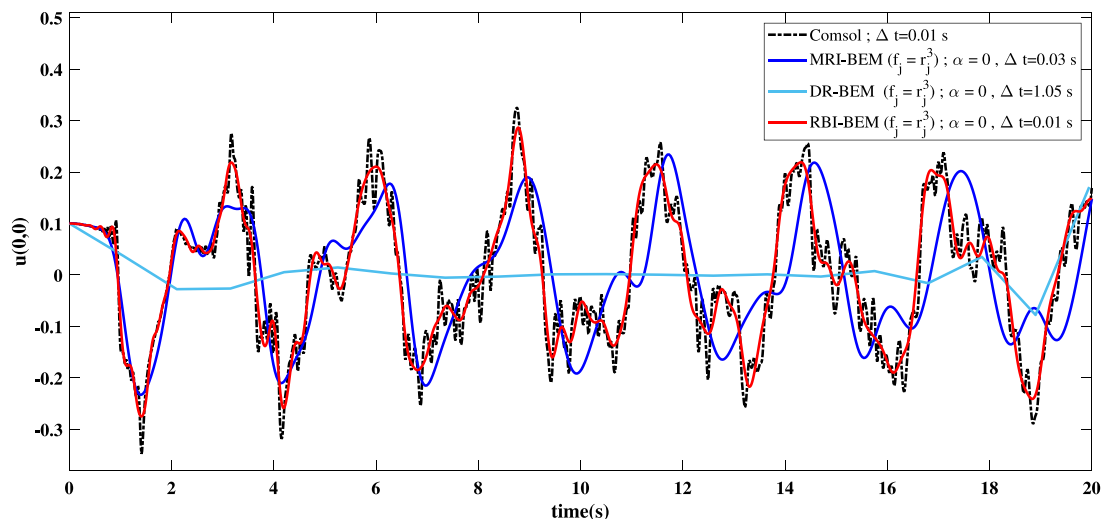


Fig. 20. Irregular domain with a smooth edge: Potential at point $A(0,0)$ with $f_j = r_j^3$ and the Houbolt- α method.

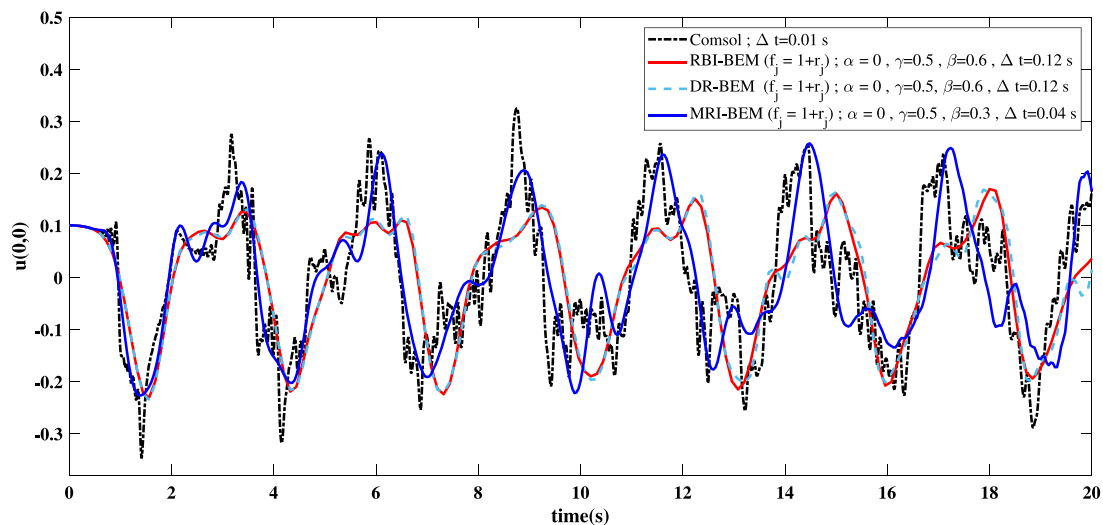


Fig. 21. Irregular domain with a smooth edge: Potential at point $A(0,0)$ with $f_j = 1 + r_j$ and the Newmark- α method.

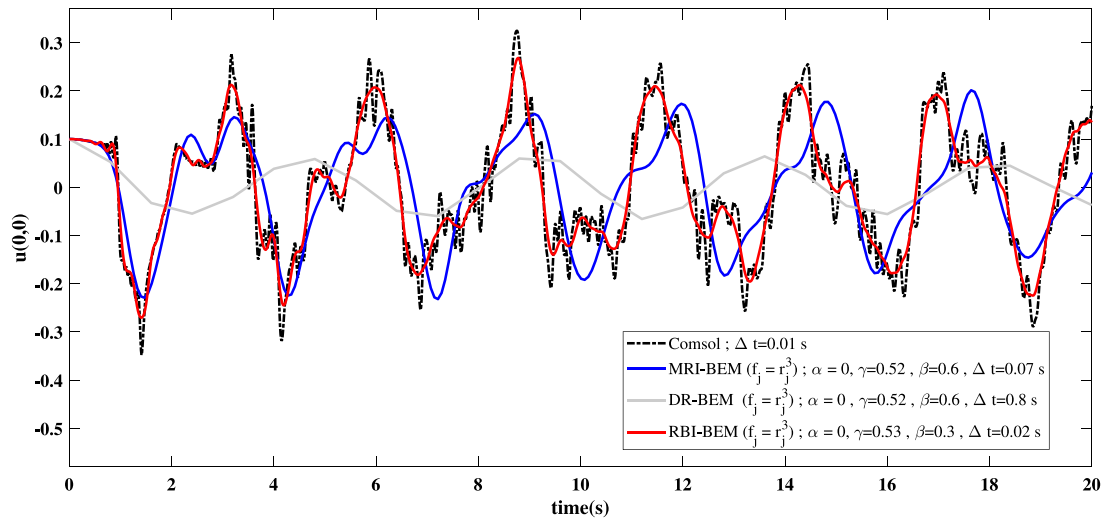


Fig. 22. Irregular domain with a smooth edge: Potential at point $A(0,0)$ with $f_j = r_j^3$ and the Newmark- α method.

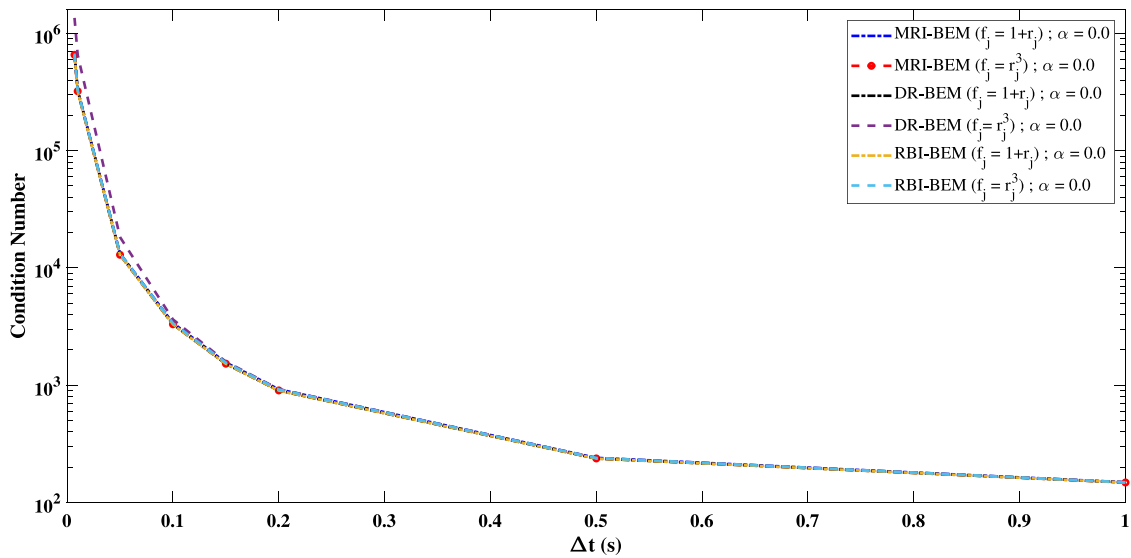


Fig. 23. Variation of condition number for matrix K vs time step using the Houbolt- α method in example 1.

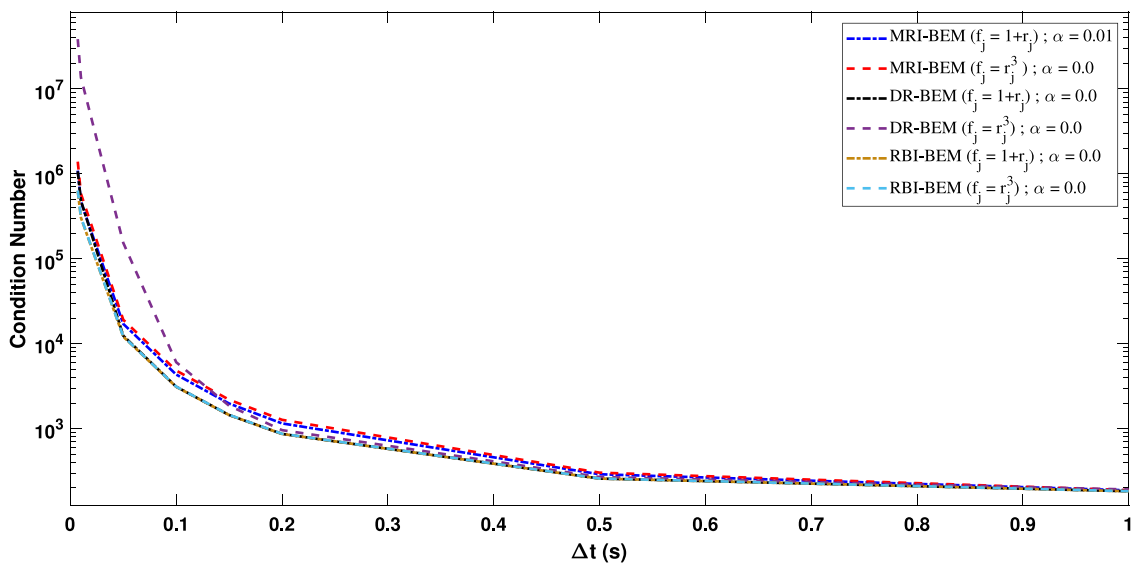


Fig. 24. Variation of condition number for matrix K vs time step using the Houbolt- α method in example 2.

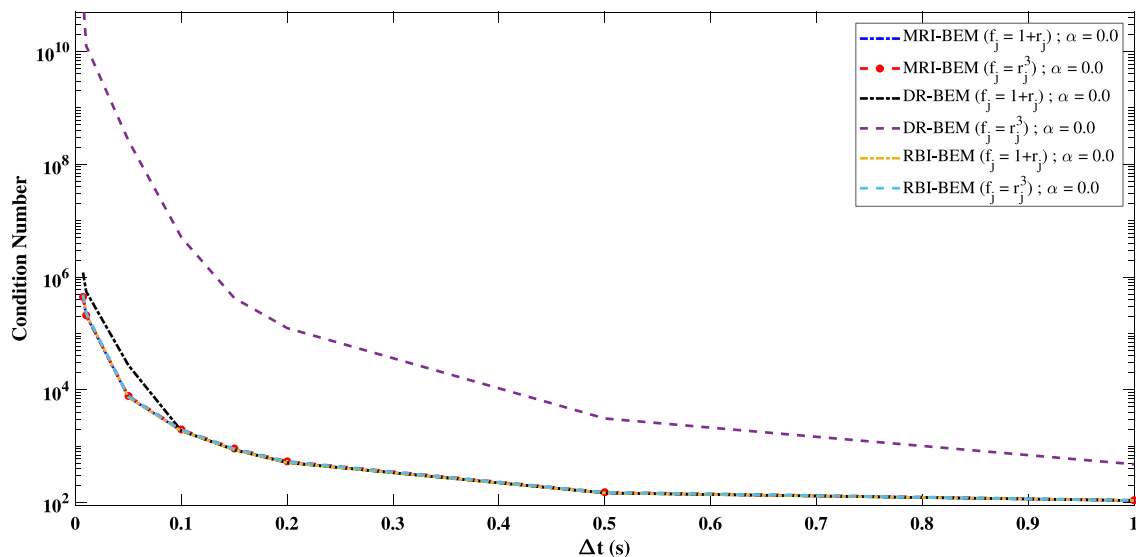


Fig. 25. Variation of condition number for matrix K vs time step using the Houbolt- α method in example 3.

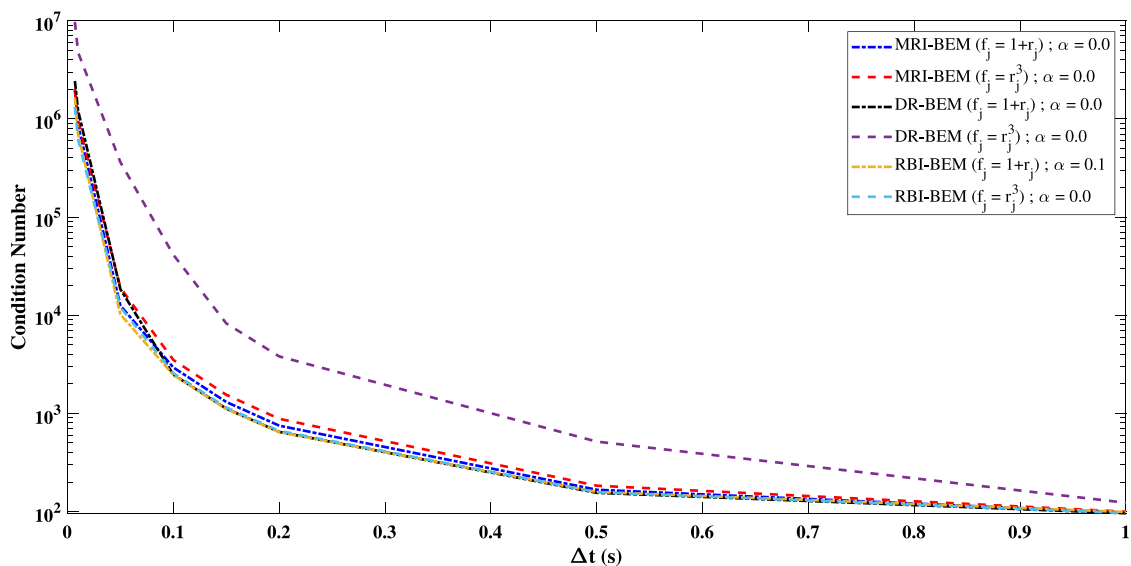


Fig. 26. Variation of condition number for matrix K vs time step using the Houbolt- α method in example 4.

Table 7
Minimum time step required for stability for all examples using Newmark- α .

f_j	Example	Approach		
		DR-BEM	MRI-BEM	RBI-BEM
$1 + r_j$	1	0.0005 s	0.0005 s	0.0005 s
	2	0.001 s	0.005 s	0.0005 s
	3	0.09 s	0.0005 s	0.0005 s
	4	0.1 s	0.04 s	0.1 s
r_j^3	1	0.0005 s	0.0005 s	0.0005 s
	2	0.07 s	0.014 s	0.0005 s
	3	0.3 s	0.0008 s	0.0005 s
	4	0.8 s	0.07 s	0.02 s

to instability issues (see Tables 6–7), since it was not possible to find a more precise or convergent solution by decreasing the time step, maintaining the same parameters of the analyzed time marching integration methods, nor making a variation of them. For this reason, only the best results were shown in this work.

It is possible to find justifications for the poor performance of DR-BEM or MRI-BEM in combination with the radial basis functions used for certain examples by reviewing the following: After substituting the boundary conditions, the resultant matrix of the system of equations is obtained, henceforth called K , which also depends on values calculated from the inverse of the interpolation matrix F . It has been observed that if the condition number of F is relatively high (which increases with the number of points used to interpolate, and it was also reported in [35]), the condition number of matrix K is also affected. In order to find out the difference between the curves obtained for the condition numbers vs the time step for the different formulations, Figs. 23–26 were plotted. There it is observed that the condition number of the matrix K varies with the value of Δt and its tendency is generally decreasing for higher values of Δt . The values of the condition numbers are similar between the different methods, except when DR-BEM and the cubic function are combined. The same behavior was observed when using Newmark- α instead. Furthermore, it is observed that the values of Δt used to obtain the lowest possible average relative error in the results for the different examples generally corresponded to the highest condition number values.

In the Tables 6–7 it can be seen that both time marching schemes can be unstable for certain time steps, possibly influenced by the ill-conditioning of the matrices (which worsens when the number of poles is significantly increased) in combination with certain inadequate radial basis function for the problem under analysis. Regarding the size of the intervals of Δt where the solution was stable, there it is also observed that with the RBI-BEM formulation the largest ranges were obtained on average, while with DR-BEM the smallest ones.

In the analysis of the different problems, there were two situations where it was not possible to achieve good results for the different approaches: The first one was when using the shortest time step within the range where there was stability. This is because that value does not necessarily coincide with the appropriate Δt according to the wave propagation speed, and therefore, the precision of the time marching method is reduced and deviated results are obtained concerning reference values. The second case occurred even when using an appropriate time step, as in the second example when using MRI-BEM. In this case, we can affirm that it may be due to the inability of such radial basis functions to adequately represent the variation of the variable to be approximated under the particular conditions of that problem (Discontinuous initial conditions for the velocity), without neglecting the effect that it can cause matrix ill-conditioning. The above can be supported by what was found in the following works:

- In [47] the Thin Plate Spline radial basis function was used in all examples because it was the only one that produced good results with the DR-BEM. Here the following is also stated: “An excessive number of poles can disturb the results, since the DR-BEM is not a simple interpolation technique and conditioning matrix problems and inadequacy of certain radial functions are related in many computational tests”.
- In [48] the function r_j^3 was proved to be unpredictable in the DR-BEM. Similarly in [49] it was found that not all RBFs are appropriate to solve a certain problem with the DR-BEM.
- In [34] it is not explained for what reasons the function r_j^3 was only used for all the examples and therefore it is not known if there are problems with the use of other functions in MRI-BEM. On the other hand, the analyzes on the influence of the number of internal points on the quality of the solution that has been made in works where MRI-BEM has been implemented, only a maximum of 66 internal points have been considered, not relatively large quantities such as the used in the second and fourth example of our work, which were 625 and 405 respectively. Although the results of other simulations were not included in the present paper, it is good to highlight that for the second example no better results were obtained with MRI-BEM when using a smaller number of internal points (125 or 441) nor when using a larger quantity (1089).
- According to [50] the DI-BEM performance was found to be sensitive to the kind of RBF used to interpolate the source term. They got the worst results using the function $1 + r_j^3$ with DI-BEM to solve a certain 3D model, while its use with DR-BEM had been a relative success in a reference paper.

7. Conclusions

In the present article, a promising domain integration quadrature-based method was used to address wave propagation problems with the boundary elements. In general, the condition number of the matrices alone is not decisive to know if good results will be obtained, since both the type of BEM formulation (DR-BEM, MRI-BEM, RBI-BEM, etc.) and the specific conditions of the problem can influence. The RBI-BEM formulation appears to be more stable when using both the linear and cubic RBFs and a relatively high quantity of internal points in comparison with the DR-BEM and the MRI-BEM ones. Other simulations not included in this work carried out with functions $f_j = r_j^2 \log(r_j)$ and $f_j =$

$r_j^4 \log(r_j)$ also produced very good results with RBI-BEM, however, the performance of the present approach could be sensitive to some types of radial basis function and therefore, it is necessary to review the stability and quality of the solutions when using other global functions or those with compact support. Which will be addressed in future research. Although the results for the function r_j^3 using both time marching schemes in the first example were not shown, all the formulations were in good agreement with the analytical solution, therefore, it is confirmed that the type of problem also influences the performance of the method used to transform the domain integral. On the other hand, by using the present approach, the weakly singular domain integrals appearing in BEM formulations may be evaluated directly without using any treatment for the integrand. The present approach lacks some limitations found in DR-BEM in relation to the choice of approximating RBFs and is less time-consuming than the MRI-BEM. It can be used to solve problems with simple or multi-connected convex and concave geometries. Both Houbolt- α and Newmark- α methods are suitable to solve this kind of problem, however, Newmark- α has a greater number of control parameters that could be helpful in certain cases. The present method may be implemented in BEM for solving several linear and nonlinear engineering problems.

Acknowledgment

The authors gratefully acknowledges the Technological University of Bolívar for supporting this work.

References

- [1] Dallner R, Kuhn G. Efficient evaluation of volume integrals in the boundary element method. *Comput Methods Appl Mech Engrg* 1993;109(1):95–109. [http://dx.doi.org/10.1016/0045-7825\(93\)90226-N](http://dx.doi.org/10.1016/0045-7825(93)90226-N), URL <https://www.sciencedirect.com/science/article/pii/004578259390226N>.
- [2] Carrer JAM, Mansur WJ, Vanzuit RJ. Scalar wave equation by the boundary element method: a D-BEM approach with non-homogeneous initial conditions. *Comput. Mech* 2009;44(1):31. <http://dx.doi.org/10.1007/s00466-008-0353-4>.
- [3] Carrer JAM, Mansur WJ. Scalar wave equation by the boundary element method: a D-BEM approach with constant time-weighting functions. *Internat J Numer Methods Engrg* 2010;81(10):1281–97. <http://dx.doi.org/10.1002/nme.2732>.
- [4] Ding J, Ye W. A grid-based integral approach for quasilinear problems. *Comput Mech* 2006;38(2):113–8.
- [5] Koehler M, Yang R, Gray LJ. Cell-based volume integration for boundary integral analysis. *Internat J Numer Methods Engrg* 2012;90(7):915–27.
- [6] Wang Q, Zhou W, Cheng Y, Ma G, Chang X, Huang Q. An adaptive cell-based domain integration method for treatment of domain integrals in 3D boundary element method for potential and elasticity problems. *Acta Mech Solida Sin* 2017;30(1):99–111. <http://dx.doi.org/10.1016/j.camss.2016.08.002>, URL <https://www.sciencedirect.com/science/article/pii/S0894916616300751>.
- [7] Nardini D, Brebbia C. A new approach to free vibration analysis using boundary elements. *Appl Math Model* 1983;7:157–62.
- [8] Partridge PW, Brebbia CA. Computer implementation of the BEM dual reciprocity method for the solution of general field equations. *Commun Appl Numer Methods* 1990;6(2):83–92. <http://dx.doi.org/10.1002/cnm.1630060204>.
- [9] Agnantiaris J, Polyzos D, Beskos D. Some studies on dual reciprocity BEM for elastodynamic analysis. *Comput Mech* 1996;17(4):270–7.
- [10] Partridge PW, Brebbia CA, et al. *Dual reciprocity boundary element method*. Springer Science & Business Media; 2012.
- [11] Useche J, Narvaez A. Vibrational response of elastic membranes coupled to acoustic fluids using a BEM–BEM formulation. In: De Clerck J, editor. *Topics in modal analysis I*, vol. 7. Cham: Springer International Publishing; 2014, p. 333–40.
- [12] Useche J. Vibration analysis of shear deformable shallow shells using the boundary element method. *Eng Struct* 2014;62–63:65–74. <http://dx.doi.org/10.1016/j.engstruct.2014.01.010>.
- [13] Useche J, Alvarez H. Elastodynamic analysis of thick multilayer composite plates by the boundary element method. *CMES-Comput Model Eng Sci* 2015;107(4):277–96.
- [14] Ochiai Y, Sladek V, Sladek J. Transient heat conduction analysis by triple-reciprocity boundary element method. *Eng Anal Bound Elem* 2006;30:194–204. <http://dx.doi.org/10.1016/j.enganabound.2005.07.010>.
- [15] Guo S, Wu Q, Li H-G, Kuidong G. Triple reciprocity method for unknown function's domain integral in boundary integral equation. *Eng Anal Bound Elem* 2020;113:170–80. <http://dx.doi.org/10.1016/j.enganabound.2019.12.014>.

- [16] Nowak A, Brebbia C. The multiple-reciprocity method. a new approach for transforming bem domain integrals to the boundary. *Eng Anal Bound Elem* 1989;6(3):164–7.
- [17] Nowak A. The multiple reciprocity boundary element method. Southampton: Computational Mechanics Publication; 1994, p. 1–41.
- [18] Ochiai Y, Sekiya T. Steady thermal stress analysis by improved multiple-reciprocity boundary element method. *J. Therm Stresses* 1995;18(6):603–20.
- [19] Ochiai Y, Sekiya T. Steady heat conduction analysis by improved multiple-reciprocity boundary element method. *Eng Anal Bound Elem* 1996;18(2):111–7.
- [20] Gao X-W. The radial integration method for evaluation of domain integrals with boundary-only discretization. *Eng Anal Bound Elem* 2002;26(10):905–16.
- [21] Loeffler C, Cruz A, Bulcão A. Direct use of radial basis interpolation functions for modelling source terms with the boundary element method. *Eng Anal Bound Elem* 2015;50:97–108. <http://dx.doi.org/10.1016/j.enganabound.2014.07.007>.
- [22] Gao X-W. Evaluation of regular and singular domain integrals with boundary-only discretization—theory and fortran code. *J Comput Appl Math* 2005;175(2):265–90.
- [23] Gipson G. The coupling of Monte Carlo integration with boundary integral techniques to solve Poisson-type problems. *Eng Anal* 1985;2(3):138–45.
- [24] Kagawa Y, Murai T. Use of Monte Carlo method for singular integral evaluation in boundary elements. *COMPEL* 1991.
- [25] Rosca VE, ao VML. Quasi-Monte Carlo mesh-free integration for meshless weak formulations. *Eng Anal Bound Elem* 2008;32(6):471–9. <http://dx.doi.org/10.1016/j.enganabound.2007.10.015>, Meshless Methods.
- [26] Hematiyan M. A general method for evaluation of 2D and 3D domain integrals without domain discretization and its application in BEM. *Comput Mech* 2007;39(4):509–20.
- [27] Narváez A, Useche J. The kriging integration method applied to the boundary element analysis of Poisson problems. *Eng Anal Bound Elem* 2020;121:1–20. <http://dx.doi.org/10.1016/j.enganabound.2020.09.001>.
- [28] Houbolt JC. A recurrence matrix solution for the dynamic response of elastic aircraft. *J Aeronaut Sci* 1950;17(9):540–50.
- [29] Newmark NM. A method of computation for structural dynamics. *J Eng Mech Div* 1959;85(3):67–94.
- [30] Yu G, Mansur WJ, Carrer JAM, Gong L. A linear θ method applied to 2D time-domain BEM. *Commun Numer Methods Eng* 1998;14(12):1171–9. [http://dx.doi.org/10.1002/\(SICI\)1099-0887\(199812\)14:12<1171::AID-CNM217>3.0.CO;2-G](http://dx.doi.org/10.1002/(SICI)1099-0887(199812)14:12<1171::AID-CNM217>3.0.CO;2-G), URL <https://onlinelibrary.wiley.com/doi/abs/10.1002/>.
- [31] Chen W, Tanaka M. A study on time schemes for DRBEM analysis of elastic impact wave. *Comput Mech* 2002;28:331–8. <http://dx.doi.org/10.1007/s00466-001-0297-4>.
- [32] Carrer J, Mansur W. Alternative time-marching schemes for elastodynamic analysis with the domain boundary element method formulation. *Comput Mech* 2004;34:387–99. <http://dx.doi.org/10.1007/s00466-004-0582-0>.
- [33] Oyarzún P, Loureiro F, Carrer J, Mansur W. A time-stepping scheme based on numerical green's functions for the domain boundary element method: The exga-DBEM newmark approach. *Eng. Anal. Bound. Elem.* 2011;35:533–42. <http://dx.doi.org/10.1016/j.enganabound.2010.08.015>.
- [34] Najjarzadeh L, Movahedian B, Azhari M. Numerical solution of scalar wave equation by the modified radial integration boundary element method. *Eng Anal Bound Elem* 2019;105:267–78. <http://dx.doi.org/10.1016/j.enganabound.2019.04.027>, URL <https://www.sciencedirect.com/science/article/pii/S095579971830701X>.
- [35] Qu S, Li S, Chen H-R, Qu Z. Radial integration boundary element method for acoustic eigenvalue problems. *Eng Anal Bound Elem* 2013;37(7):1043–51. <http://dx.doi.org/10.1016/j.enganabound.2013.03.016>.
- [36] AL-Jawary MA, Wrobel LC. Numerical solution of the two-dimensional Helmholtz equation with variable coefficients by the radial integration boundary integral and integro-differential equation methods. *Int J Comput Math* 2012;89(11):1463–87. <http://dx.doi.org/10.1080/00207160.2012.667087>.
- [37] Campos LS, Loeffler CF, Netto FO, de Jesus dos Santos A. Testing the accomplishment of the radial integration method with the direct interpolation boundary element technique for solving Helmholtz problems. *Eng Anal Bound Elem* 2020;110:16–23. <http://dx.doi.org/10.1016/j.enganabound.2019.09.022>.
- [38] Gandomkar M, Dibajian S, Farzin M, Hashemolhoseini S. An integration procedure for meshless methods using kriging interpolations. *Indian J Sci Technol* 2013;6(1):3859–67.
- [39] Wrobel LC. Boundary element method, volume 1: Applications in thermo-fluids and acoustics, vol. 1. John Wiley & Sons; 2002.
- [40] Katsikadelis JT. The boundary element method for engineers and scientists. 2nd Ed.. Oxford: Academic Press; 2016.
- [41] Slak J, Kosec G. On generation of node distributions for meshless PDE discretizations. *SIAM J Sci Comput* 2019;41. <http://dx.doi.org/10.1137/18M1231456>.
- [42] Gu Y, Wang Q, Lam K. A meshless local kriging method for large deformation analyses. *Comput Methods Appl Mech Engrg* 2007;196(9–12):1673–84.
- [43] Wang J, Liu G. On the optimal shape parameters of radial basis functions used for 2-D meshless methods. *Comput Methods Appl Mech Engrg* 2002;191(23–24):2611–30.
- [44] Punzi A, Sommariva A, Vianello M. Meshless cubature over the disk using thin-plate splines. *J Comput Appl Math* 2008;221(2):430–6. <http://dx.doi.org/10.1016/j.cam.2007.10.023>, URL <https://www.sciencedirect.com/science/article/pii/S0377042707005742>, Special Issue: Recent Progress in Spline and Wavelet Approximation.
- [45] Najjarzadeh L, Movahedian B, Azhari M. Stability analysis of the thin plates with arbitrary shapes subjected to non-uniform stress fields using boundary element and radial integration methods. *Eng Anal Bound Elem* 2018;87:111–21. <http://dx.doi.org/10.1016/j.enganabound.2017.11.010>.
- [46] Young D, Gu M, Fan C. The time-marching method of fundamental solutions for wave equations. *Eng Anal Bound Elem* 2009;33(12):1411–25. <http://dx.doi.org/10.1016/j.enganabound.2009.05.008>, URL <https://www.sciencedirect.com/science/article/pii/S0955799709001374>, Special Issue on the Method of Fundamental Solutions in honour of Professor Michael Golberg.
- [47] Loeffler C, Mansur W, Barcelos H, Bulcão A. Solving Helmholtz problems with the boundary element method using direct radial basis function interpolation. *Eng Anal Bound Elem* 2015;61:218–25. <http://dx.doi.org/10.1016/j.enganabound.2015.07.013>.
- [48] Uğurlu B. A dual reciprocity boundary element solution method for the free vibration analysis of fluid-coupled kirchhoff plates. *J Sound Vib* 2015;340:190–210. <http://dx.doi.org/10.1016/j.jsv.2014.12.011>.
- [49] Chanthawara K, Kaennakham S, Toutip W. The numerical study and comparison of radial basis functions in applications of the dual reciprocity boundary element method to convection-diffusion problems. 1705, 2016, 020029. <http://dx.doi.org/10.1063/1.4940277>,
- [50] Barbosa J, Loeffler C, Lara L. The direct interpolation boundary element technique applied to three-dimensional scalar free vibration problems. *Eng Anal Bound Elem* 2019;108:295–300. <http://dx.doi.org/10.1016/j.enganabound.2019.09.002>.